Distribution of Frequencies of Spontaneous Oscillations in Hair Cells of the Bullfrog Sacculus

D. Ramunno-Johnson, C. E. Strimbu, L. Fredrickson, K. Arisaka, and D. Bozovic*
Department of Physics and Astronomy and California Nanosytems Institute University of California, Los Angeles, California 90095

ABSTRACT Under in vitro conditions, free-standing hair bundles of the bullfrog (*Rana catesbeiana*) sacculus have exhibited spontaneous oscillations. We used a high-speed complementary metal oxide semiconductor camera to track the active movements of multiple hair cells in a single field of view. Our techniques enabled us to probe for correlations between pairs of cells, and to acquire records on over 100 actively oscillating bundles per epithelium. We measured the statistical distribution of oscillation periods of cells from different areas within the sacculus, and on different epithelia. Spontaneous oscillations exhibited a peak period of 33 ms (+29 ms, −14 ms) and uniform spatial distribution across the sacculus.

INTRODUCTION

Hair cells of the inner ear can detect mechanical displacements as small as a few Å (1–3). This acuity is crucially dependent on an underlying active process (4–19), whereby cells work to sustain oscillations in a viscous environment, amplify low-intensity stimuli, and exhibit spontaneous motility. Details of the active process, particularly the amplification, frequency selectivity, and mechanisms by which the system controls its gain and tuning, are subjects of ongoing study.

Hair cells of in vitro epithelial preparations excised from the bullfrog sacculus were shown to exhibit spontaneous oscillations (20–24). Their observed amplitudes can be as large as 100 nm, significantly exceeding those of thermal fluctuations, which are typically ~2 nm at ambient temperatures. Previous studies demonstrated that oscillating bundles perform work against an external load (25,26) on a cycle-by-cycle basis. Furthermore, their dynamics were compared with predictions based on the fluctuation-dissipation theorem (27), to demonstrate that they require an active mechanism and cannot be explained by a passive nonlinear process. In the context of nonlinear dynamics, the phenomenon was interpreted to indicate a system that has crossed a Hopf bifurcation, exhibiting a stable limit-cycle oscillation (28–32). An analogy often refers to an electronic amplifier with an internal positive-feedback mechanism: if the gain is increased to the point of instability, the system bursts into spontaneous oscillation.

A number of experiments probed the cellular mechanisms underlying spontaneous oscillation, and theoretical modeling captured the main features of the cycle (33–36). Nonlinearity in hair-bundle mechanics arises primarily from the transduction complex itself: mechanically sensitive ion channels open and close in response to stereociliary deflection (37–48). According to the gating-spring model, tip links (49,50) connecting adjacent stereocilia relax upon the opening of a channel, inducing a change in the effective stiffness of the hair bundle. The mechanical gating introduces a nonlinearity in the hair-cell response, and causes it to flicker between a state with most of the channels open and one with most channels closed. Meanwhile, an array of myosin motors (51–62) mediates an adaptation process in the stereocilia of a hair bundle (63–73). These molecular motors are connected to the transduction complex, and adjust tension in the attached tip link by slipping and climbing along actin filaments. A bistable system in conjunction with an adaptation mechanism exhibits spontaneous oscillation.

Although the cellular mechanisms behind spontaneous oscillations are fairly well understood, a number of questions remain in regard to their role in the active process operant in vivo. Hair bundles that exhibit oscillations are free-standing, with the overlying otolithic membrane removed by enzymatic digestion. The native mechanical load is therefore significantly changed, potentially perturbing the oscillation frequency and pushing the system into a nonphysiological regime. For this study, we obtained a statistical characterization of these oscillations, to compare them with previous measurements in this field that were performed on intact sacculi under in vivo conditions.

Firstly, we examine how spontaneous oscillation frequencies in individual hair cells compare with spontaneous spiking rates that other groups measured in auditory fibers innervating the sacculus (74,75). Under in vivo conditions, the spontaneous activity of these nerves fell in a range of 10–40 spikes/s, with a peak of ~30 spikes/s (76). Secondly, tuning curves obtained from auditory nerve fibers (77–82) in the bullfrog sacculus were shown to be quite broad, exhibiting quality factors of Q_{10dB} ~0.5–1.0 (76). We explore whether oscillations in free-standing hair bundles of an in vitro preparation display comparable quality factors, or whether individual free-standing oscillators are more sharply tuned. If the latter outcome proved true, the broadening observed in vivo may have been attributable to the nature of coupling between cells in the intact endorgan. Thirdly,

Submitted July 24, 2008, and accepted for publication September 22, 2008.

*Correspondence: bozovic@physics.ucla.edu

Editor: Alberto Diaspro.

0006-3495/09/02/1159/10 $2.00

doi: 10.1016/j.bpj.2008.09.060

the sacculus was shown to be nontonotopic, with a uniform distribution of characteristic frequencies. We inquire whether spontaneous oscillations likewise exhibit a uniform distribution by measuring both the local and global variation in their frequencies across the sacculus. By performing a systematic comparison, we assess whether spontaneous oscillations observed in free-standing hair bundles display properties comparable to those of an intact sacculus, and if they are indicative of a physiologically relevant active process.

For this purpose, it was desirable to obtain significant statistics on oscillation properties from each sacculus. Because the lifetime of a typical in vitro preparation is ~1 h, measuring oscillations from many cells requires the ability to record a number of them in parallel. We hence replaced the traditional photodiode detector, used for individual hair-bundle studies, with a high-speed complementary metal oxide semiconductor (CMOS) camera. Providing megapixel resolution, this technique allows for the parallel tracking of 10–20 cells. Simultaneous multiple-element measurement enables the accumulation of statistics as well as probing for correlations among nearby cells, a technique that can be readily generalized to further studies in the field.

METHODS

Experimental preparation

Experiments were preformed on sacculi excised from the inner ears of adult bullfrogs (*Rana catesbeiana*). For each sacculus, after a 35-min exposure to 67 μg/mL protease at room temperature, the otolithic membrane was removed, and the epithelium was placed in a two-compartment chamber (83). The bottom compartment was filled with oxygenated artificial perilymph containing 110 mM Na^+, 2 mM K^+, 1.5 mM Ca^{2+}, 118 mM Cl^-, 3 mM D-glucose, 1 mM sodium pyruvate, 1 mM creatine, and 5 mM HEPES, at a pH of 7.3 and osmolarity of ~230 mmol/kg. The apical surface was bathed with oxygenated artificial endolymph containing 117.5 mM K^+, 2 mM Na^+, 0.25 mM Ca^{2+}, 118 mM Cl^-, 3 mM D-glucose, and 5 mM HEPES, at a pH of 7.3 and osmolarity of ~230 mmol/kg. The chemical compositions of these standard artificial solutions were developed in the field to approximate physiological conditions.

Measurement

Hair bundles were imaged with an Olympus BX51WI microscope (Olympus America, San Diego, CA) with white-light transmission illumination provided by an X-Cite 120 metal halogenide lamp. We used a ×20 water-immersion objective (XLUMPLFL20XW, Olympus America) with a numerical aperture of 0.95, with further magnification provided by a double-gauss variable-focus lens, for a total magnification of ~×385. To minimize mechanical noise, the microscope was mounted on a vibration-isolation table (Technical Manufacturing, Peabody, MA) inside an acoustically isolated chamber (Industrial Acoustic, New York, NY). All images of hair-bundle oscillations were recorded with a CMOS camera (Photron FASTCAM SA1.1, Photron, San Diego, CA) containing 1024 × 1024 pixels, each 20 μm in size and with 12-bit depth. Because a single CMOS chip includes many readout channels operating in parallel, acquisition rates can be orders of magnitude higher than with traditional CCD devices. High frame rates, and hence short exposure times, require increased illumination to yield a sufficient photon count per pixel (84). The illumination provided by the X-Cite light source, coupled with the parallel readout of the CMOS chip, readily allowed recording at 500 frames per second, a temporal resolution sufficient for the purposes of this study. Because the camera can acquire megapixel images at 5400 frames per second, and proportionally higher rates at lower resolution, our method can be generalized for higher-speed recording.

To prevent degradation of the biological sample, we kept the overall duration of the experiments to ~20 min, significantly below the lifetime of a typical preparation (~45 min). We verified that exposure to incident light had no effect on oscillations over these timescales by observing that sequential recordings of bundles yielded no consistent trends of increasing or decreasing frequencies.

The spatial scale of the image projected onto the camera chip was calibrated by viewing a 600-line pair per millimeter Ronchi ruling, yielding 52 nm per pixel. Data were obtained from three regions of the sacculus. Two sets of measurements were performed on the region of the sacculus farthest from the saccular nerve. The third set was focused on the striolar region.

Analysis

Motion tracking

To extract the motion of a hair cell as a function of time, we developed software in MATLAB (The MathWorks, Natick, MA) to determine the position of the stereociliary bundle in each frame of the video record. Because the width of a pixel corresponded to 52 nm in our optical system, precision better than one tenth of a pixel was required. Applying standard procedures of superresolution imaging (85), we fit Gaussian distributions to the intensity profiles of hair bundles, to extract the center position in each frame. Incident illumination from our light source provided sufficient contrast to allow this fit to yield center positions within a noise floor of 3–5 nm.

Each video record was 1.364 s long, or 682 frames. A bandpass filter was applied to the first image, and a one-dimensional fitting window was manually selected to match the width of a hair bundle, typically ~20 pixels wide. Because the largest stereociliary deflections never exceeded two pixels, the peak position remained localized within the defined window. In each frame, the window was then centered around the brightest pixel. A Gaussian distribution, $G(x) = Ae^{-(x-\mu)^2/B}$, was then fit to the unfiltered intensity profile, locating the center position of the brightest point within the hair bundle (Fig. 1). Previous measurements in the field demonstrated that the stereocilia move in unison during oscillation, thus maintaining the shape of the bundle (86).

Time-dependent records of bundle displacement were obtained by plotting the center position extracted for each frame of the record. To improve the resolution of the trace further, three vertically adjacent pixel rows on the same bundle were tracked and averaged. Hair-bundle movements were tracked along the horizontal axis only. Because there was some distribution of bundle orientations in any given screen, this projection necessarily yielded a slight underestimate of the amplitudes of oscillation. For this study, we did not correct for this projection, because it did not affect the measured quantity, i.e., the frequency of oscillation. Positive displacement in the traces shown corresponds to movement toward the tallest stereocilia, i.e., that of channel opening, consistent with the standard convention in the literature.

Frequency determination

We analyzed oscillations in the time domain to determine the statistical distribution of the period of oscillation for each hair cell. The biphasic profile of a typical cycle facilitated this approach, because it contained sharp movements corresponding to the sudden opening and closing of transduction channels. We developed software in MATLAB (described below) to detect these transitions, determine the time intervals between them, and construct histograms to show their distribution.

Our software procedures first applied a low-pass filter to the data and identified the local maxima and minima in the trace, using standard MATLAB functions. Between adjacent extrema, a numerical derivative was applied to the record to identify the inflection points that constitute the transition times when a cell's transduction channels open or close in a concerted

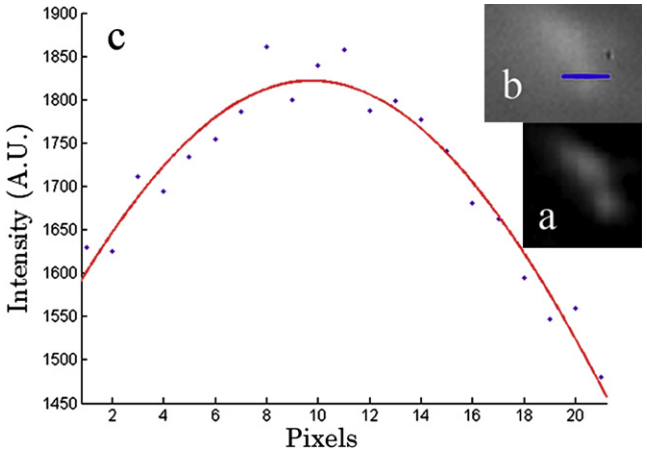

FIGURE 1 (*a*) Image of one hair bundle after bandpass filter was applied to enhance its contrast. This image served as a visual aid to facilitate selection of the feature to be tracked. (*b*) Blue line superimposed on unfiltered image indicates linear cross section used to fit the data. (*c*) Gaussian distribution (*red line*) was fit to intensity profile (*blue dots*) through the section in *b*. Center of Gaussian fit yielded the position of the bundle in a given frame.

fashion. Time intervals in the open state corresponded to the time between the opening (positive deflections) and subsequent closing (negative deflections) of channels, and time intervals in the closed state corresponded to those between closing and opening. Histograms were computed separately for the open and closed intervals, and for the combined data set. Because typical transition times were ~4 ms, this was the chosen bin size for the histograms.

Not all cells exhibited spontaneous oscillations. In the preparations used in this study, 30–70% of cells oscillated in each field of view. Among spontaneously moving bundles, ~15% were excluded from the analysis, because traces were too noisy to allow unambiguous transition assignment. In total, 373 spontaneously oscillating bundles were measured for this experiment.

The probability density estimator was shown in the literature to provide a more accurate representation of data than the traditional histogram, and is less sensitive to the chosen bin size. We applied this estimator (kernel density estimator in MATLAB) to obtain a continuous probability distribution of the half-period of oscillation, computed from data pooled over all spontaneously oscillating cells within a given screen. The peak of the dominant mode of the distribution and its full width at half maximum (FWHM) were computed for each field of view.

Imaging the sacculus

For each sacculus, records were obtained in 16 fields of view localized to a particular area of the epithelium. Fields of view were chosen with sufficient overlap to enable their relative alignment. The positions of cells visible in more than one screen were used to determine the relative offset needed to construct a tiled image of the records.

Correlation coefficients

In selected screens, the correlation coefficient was computed for each pair of hair bundles captured within that field of view. The correlation coefficient was defined as:

$$C_{X,X_2} = \frac{\mathrm{cov}(X, X_2)}{\sigma_X \sigma_{X_2}},$$

$$\mathrm{cov}(X, X_2) = \big\langle (X - \langle X \rangle)(X_2 - \langle X_2 \rangle) \big\rangle,$$

where X and X_2 denote positions of the two bundles, and σ_X and σ_{X_2} denote standard deviations.

RESULTS

Imaging the epithelium with a high-speed CMOS camera allowed for the simultaneous recording of 10–20 hair bundles per field of view (Fig. 2). Deflection of a hair bundle as a function of time was determined by extracting its center position in each frame of the record. As seen in the traces, the achieved spatial resolution was comparable to that obtained in previous measurements with a dual-photodiode detector (23,26,83), with typical noise floors on the order of 3–5 nm.

Spontaneous oscillation periods

Movements of hair bundles follow the dynamics of a relaxation oscillation, with a characteristic biphasic waveform (24,27,31): sharp transitions, indicative of the opening and closing of transduction channels, are followed by a slow exponential movement, corresponding to slipping and climbing of the myosin-motor complex. Unlike an ideal limit-cycle oscillation, however, spontaneous oscillations exhibited by hair bundles of the bullfrog sacculus display significant noise. Apart from the thermal jitter superimposed on the cycle, fluctuations occur in the local frequency and phase of the oscillation, with sporadic pauses of over 100 ms between periodic movements. Insofar as a single frequency could not be assigned to each hair cell, we performed a statistical assessment of their oscillations. We measured the time intervals between consecutive openings and closings of transduction channels. Fig. 3 shows typical traces of bundle oscillations, with the detected transitions superimposed. Probability distributions of extracted time

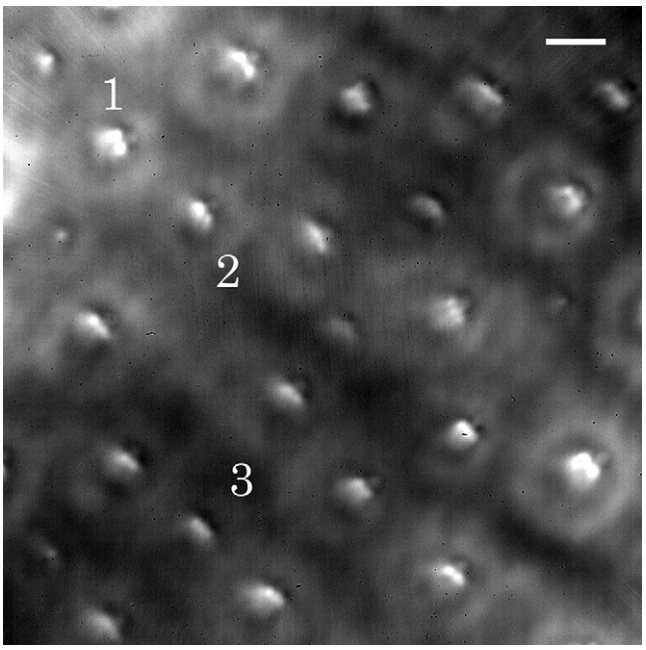

FIGURE 2 Top-down view of hair bundles of sacculus, with otolithic membrane removed by enzymatic digestion. Image shows first of 700 frames from a typical video record. Scale bar equals 5 μm.

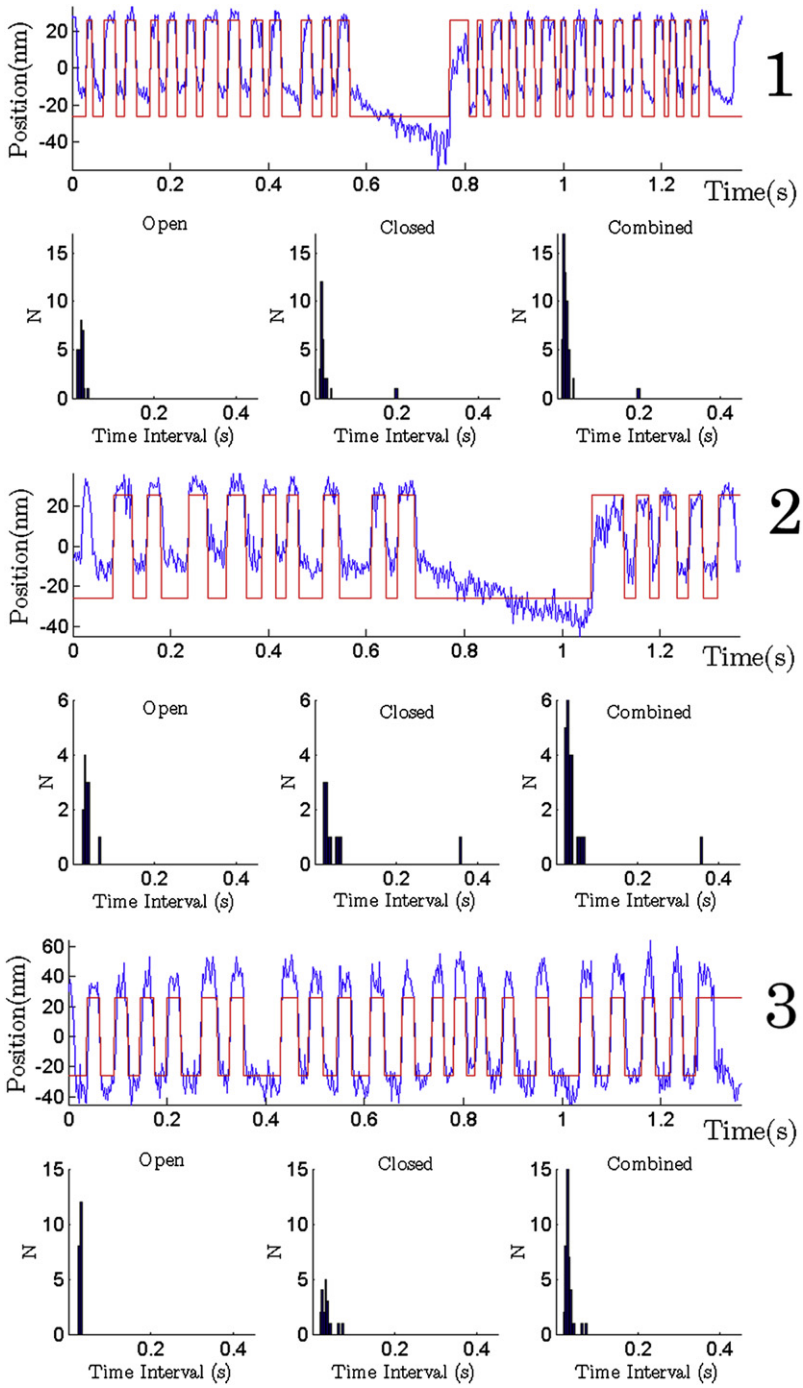

FIGURE 3 Traces of bundle motion as a function of time (*blue lines*) for three selected cells in a field of view (image shown in Fig. 2). Red line overlaid atop trace indicates times corresponding to concerted opening and closing of transduction channels. Time intervals in open states (positive deflection) and closed states (negative deflection) are determined from the record, and histograms of their distribution are shown (*left* and *middle*) below traces. Time intervals in open and closed states were combined in histograms (*right*) below each trace. Bin size was 4 ms.

intervals in the open and closed states are given in the histograms below the traces. Within each field of view, no consistent trends or spatial patterns were evident in the distribution of oscillation periods of individual bundles.

The measured time intervals were then pooled over the population of all spontaneously oscillating bundles imaged within a given screen (Fig. 4). To assess potential differences between intervals separating the opening and closing of channels (positive deflection) and those between closing and opening (negative deflection), we plotted these differences in separate histograms. Whereas the open and closed distributions displayed significant differences in the tail region of the histograms, the peaks of dominant modes fell within the same range. Hence, for the purposes of this study, we used the combined data from open and closed states to analyze the distribution of half-periods of the oscillation of hair bundles in each field of view.

Long tails were frequently evident in the probability distributions of these time intervals, corresponding to sporadic pauses apparent in the spontaneous oscillations of a cell. These

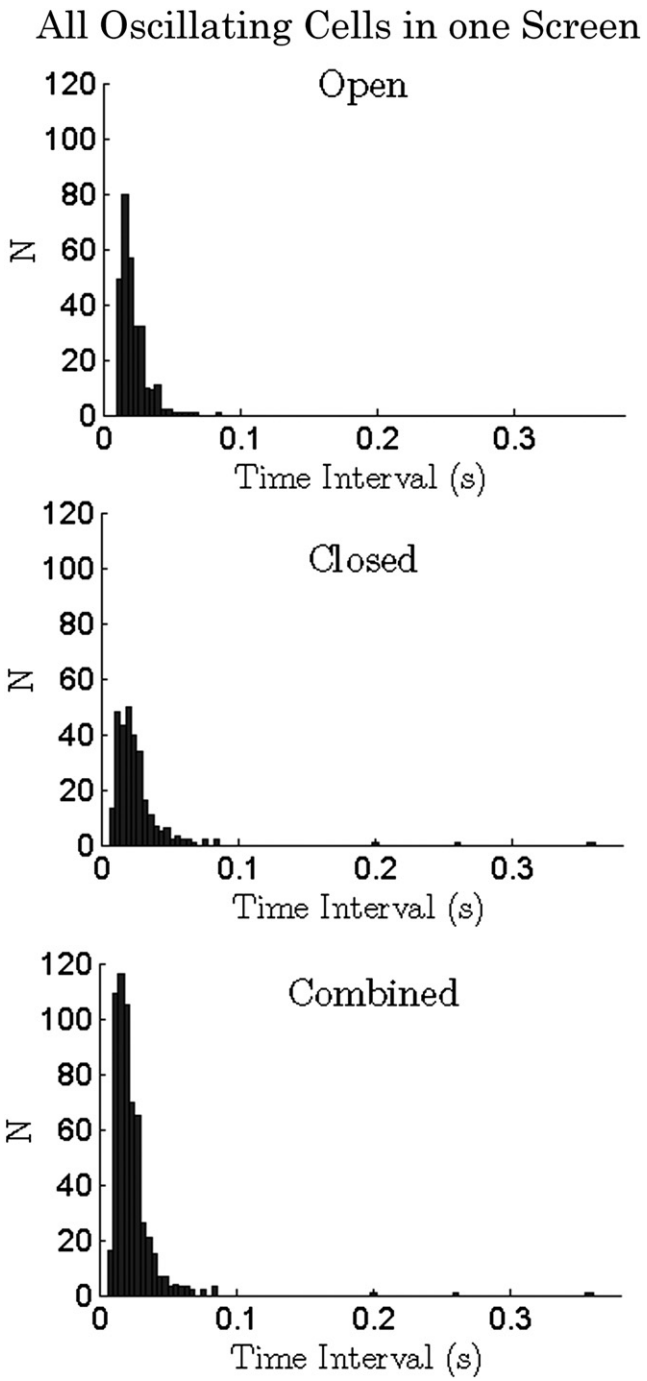

FIGURE 4 Histograms of time intervals in open (*top*) and closed (*middle*) states pooled from all oscillating cells in one field of view. Combined distribution of open and closed intervals is also shown (*bottom*).

occurred mostly in the closed state of a bundle, corresponding to deflection in the negative direction. In this study, we focused on the dominant modes of probability distributions.

Comparison of oscillations across the sacculus

Our imaging technique allowed us to explore a broader area of the epithelium, scanning typically 16 screens of 52 × 52 μm^2 each. Individual screens were offset with sufficient overlap to allow for alignment into a mosaic image (Fig. 5) of the measured portion of a sacculus.

For each screen of the epithelium shown in Fig. 5, the probability density estimator was applied to the measured time intervals pooled from all oscillating cells (Fig. 6). Peaks and FWHMs of the main mode were extracted for the probability distribution in each field of view, and are shown geometrically in Fig. 7 (see also Table 1). The center radius of each annulus in Fig. 7 indicates the peak period of oscillations, and the inner and outer radii denote the FWHM. The distribution of oscillation periods did not reveal any spatial dependence or consistent trends. The peak of the mode extracted for each individual screen fell within the FWHM of the modes determined for all other screens. Typical ratios ($\frac{T_0}{\Delta T}$) were in the range of 0.57–1.4. The histogram in Fig. 8 (*middle*) displays data pooled from all 16 fields of view measured in this epithelium. The pooled data contained the same statistical characteristics as data obtained from individual screens. Consistent distributions were therefore evident over several hundred microns of the sensory epithelium.

The main morphological feature of the distribution of cells within the sacculus is the existence of a striola (35,87), a virtual line dividing hair bundles of opposite orientations. Above the striola, the tallest stereocilia point toward the top rim of the epithelium (upward, in the images shown). Below the striola, they point toward the bottom rim. To

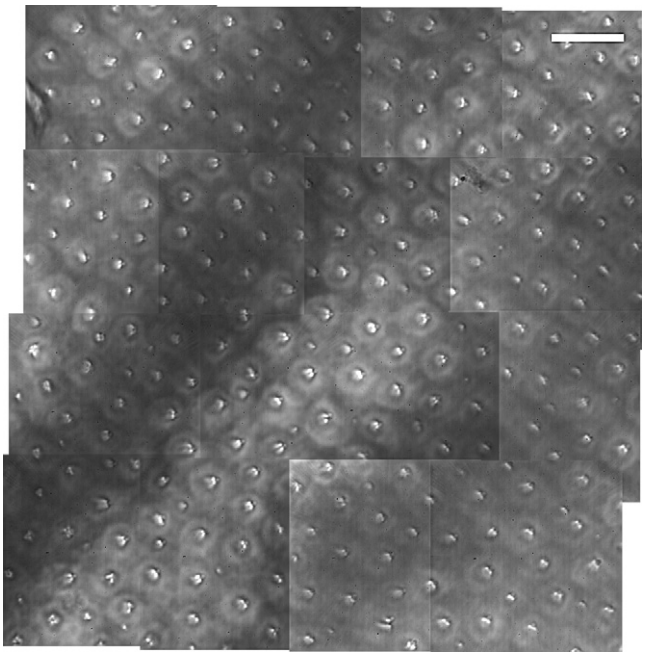

FIGURE 5 Sixteen fields of view were recorded from an area near outer edge of saccular epithelium. Overlap between adjacent records allowed for their relative alignment and formation of a mosaic image of this section of the preparation. Scale bar equals 20 μm.

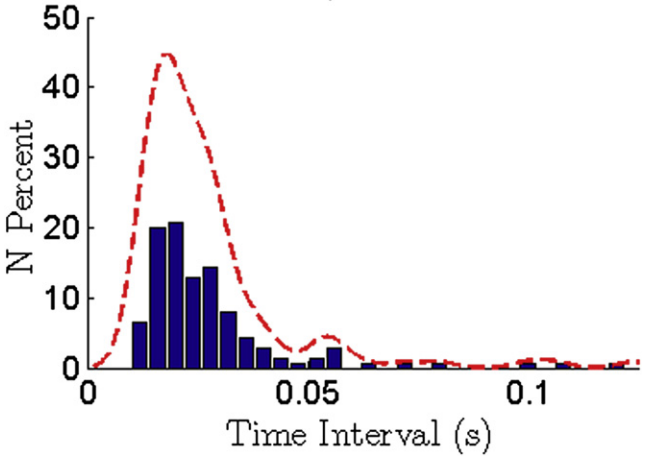

FIGURE 6 Probability density estimator was applied to compute continuous distribution (*red dashed line*) of half-period of oscillation. Time intervals measured in open and closed states were pooled over all oscillating hair bundles within a selected field of view (epithelium shown in Fig. 5). A histogram plot of same data set is shown in graph (*blue*). Two representations of the probability distribution were independently normalized.

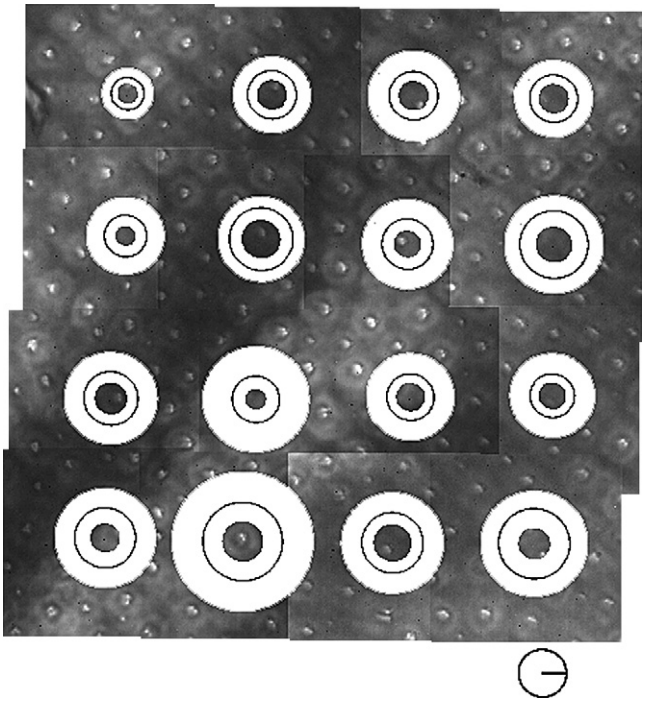

FIGURE 7 Tiled image of epithelium in Fig. 5 is reproduced, with distribution of periods of oscillation superimposed atop each screen. Geometric representation gives center and spread of oscillation periods for each field of view. The radius of the black circle within each annulus represents the peak period for that screen. The inner and outer radii defining the annulus represent the two points delimiting the FWHM of the probability distribution. The radius of the scale bar equals 30 ms.

explore whether this feature has any correlation with frequencies of spontaneous oscillation, we scanned a region surrounding the striola, capturing within the same screen hair bundles oriented in opposite directions. Fig. 9, presents an example of such a recording, where the probability distributions were computed for data separately pooled over groups of cells displaying opposite orientations. The two areas continued to show consistency in the distribution of half-periods of oscillation, indicating that the striolar region neither differs from other areas of the epithelium nor acts to separate regions of different frequencies.

To verify uniformity further in the distribution of oscillation periods, we repeated these measurements at different points in the sacculi, in different preparations, and on bullfrogs obtained from different providers. Fig. 8 depicts histograms of time intervals measured in three different epithelia, with schematic diagrams of sections within the sacculus from which the data were obtained. For each of these experiments, ~16 screens were recorded, covering an area comparable to that shown in Fig. 5. Fig. 10 provides data pooled over all three of these measurements. The combined histogram, with cells measured over many preparations, illustrates the consistency of the statistical trends measured. We conclude that the distribution of periods of spontaneous oscillation is uniform across the epithelium, with a peak at 33 ms (+29 ms, −14 ms).

Distribution of oscillation frequencies

To facilitate comparisons with other studies in the field, we converted the measured peaks in the probability distribution from time to frequency domain. For each screen of the epithelium shown in Fig. 5, we applied the probability density estimator to obtain a distribution of oscillation periods for the group of cells within the field of view. The peak frequencies, defined as the inverse of the peak periods, fell in a range of 19–46 Hz in this preparation.

Absence of correlations of nearby oscillators

To verify that each free-standing hair bundle oscillates independently, we computed correlation coefficients between all pairs of bundles in a field of view. The scatterplot of these coefficients as a function of the distance between cells is given in Fig. 11, along with a histogram of their distribution. No correlation was evident in our recordings, indicating an absence of any intrinsic entrainment.

TABLE 1 Distribution of oscillation half-periods

	Column 1	Column 2	Column 3	Column 4
Row 1	19 ms + 32 ms − 11 ms	33 ms + 18 ms − 12 ms	33 ms + 27 ms − 12 ms	32 ms + 19 ms − 11 ms
Row 2	28 ms + 22 ms − 14 ms	42 ms + 15 ms − 15 ms	34 ms + 26 ms − 15 ms	46 ms + 19 ms − 20 ms
Row 3	36 ms + 25 ms − 14 ms	31 ms + 38 ms − 17 ms	31 ms + 26 ms − 11 ms	29 ms + 26 ms − 10 ms
Row 4	40 ms + 25 ms − 20 ms	53 ms + 40 ms − 25 ms	41 ms + 26 ms − 15 ms	47 ms + 23 ms − 25 ms

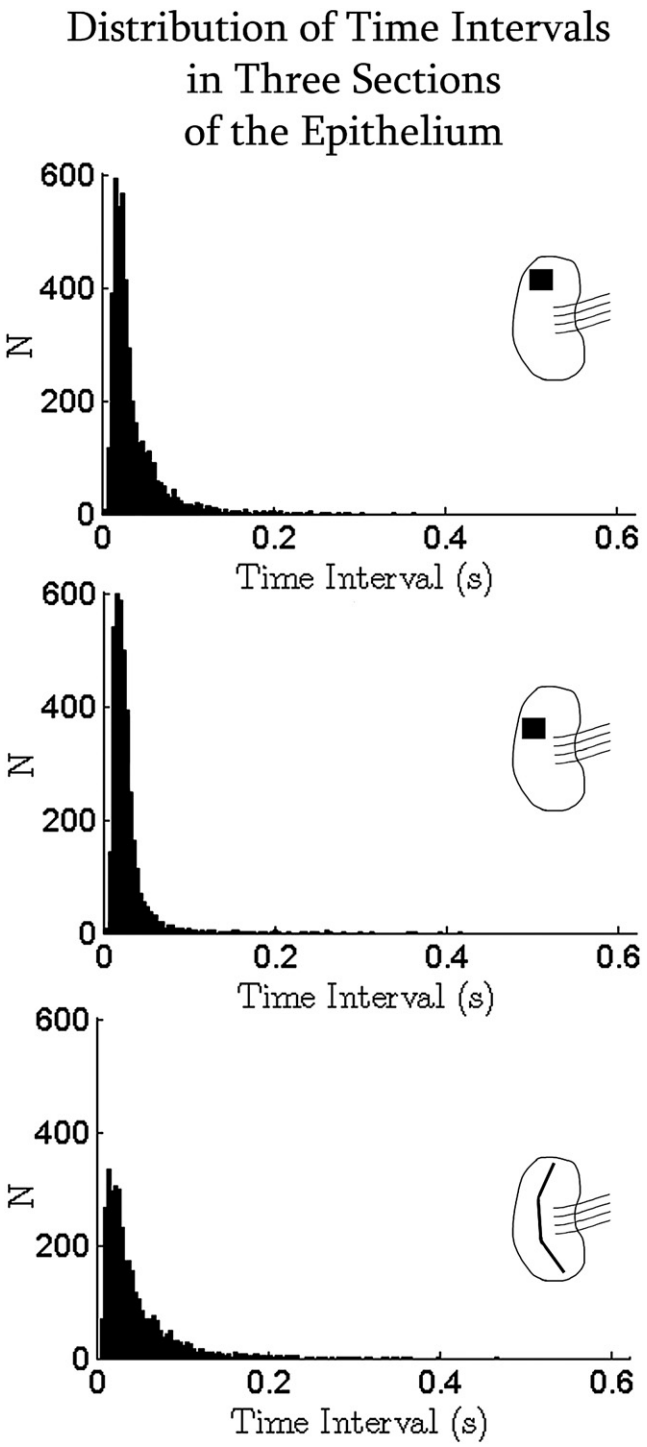

FIGURE 8 Each histogram displays distribution of data pooled over all oscillating cells measured in a given epithelium. Combined time intervals in open and closed states were used, representing half a period of oscillation. Panels represent data obtained from different sections of sacculi, extracted from inner ears of different bullfrogs. Histograms (*top* and *middle*) represent areas of sacculus close to outer edge of epithelium, and histogram at bottom represents an area along the striola. (*Insets*) Schematic diagrams show locations within sacculus where measurements were performed. Distribution in the middle was obtained from the preparation depicted in Fig. 5.

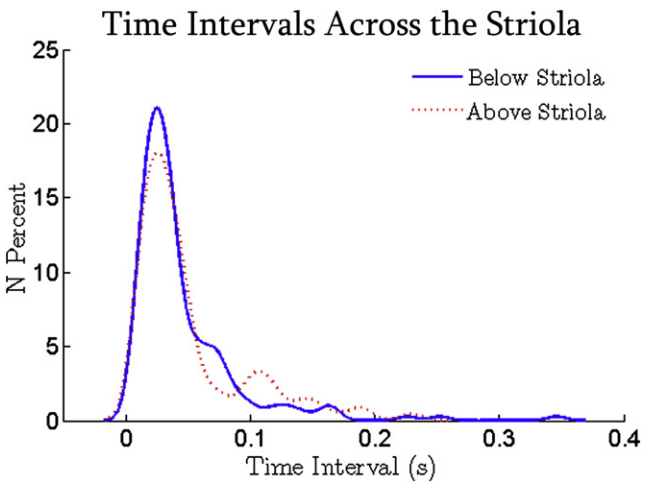

FIGURE 9 Distribution of time intervals measured from cells surrounding striolar region. Probability density estimator was applied to data pooled from all cells in a field of view oriented in one direction (above striola), and separately computed for cells displaying opposite orientation (below striola). Two curves were independently normalized to unity.

DISCUSSION

A number of in vivo studies thoroughly characterized the behavior of an intact sacculus (74–82). Tuning curves, measured in auditory nerve fibers connecting to the sacculus, exhibited the best frequencies, in a range of 20–120 Hz. Resting spike rates measured in the fibers were shown to peak at ~30 spikes/s. Finally, quality factors of 0.5–1.0 demonstrated that the sacculus is a broadly tuned organ, apparently optimized for sensitivity rather than for frequency-selectivity of detection. Although establishing direct connections between movements of individual cells and the behavior of an intact organ is not yet possible, we explored the consistency between the two by performing a statistical study of hair-bundle motion. We focused on

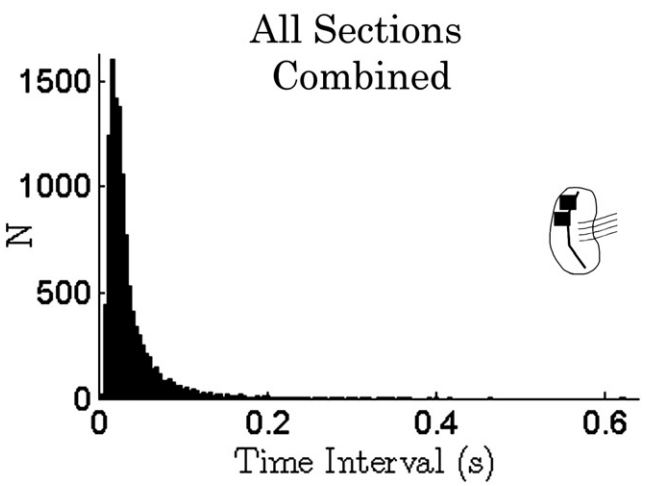

FIGURE 10 Histogram shows distribution of time intervals pooled from data obtained from all three preparations, displayed separately in Fig. 8.

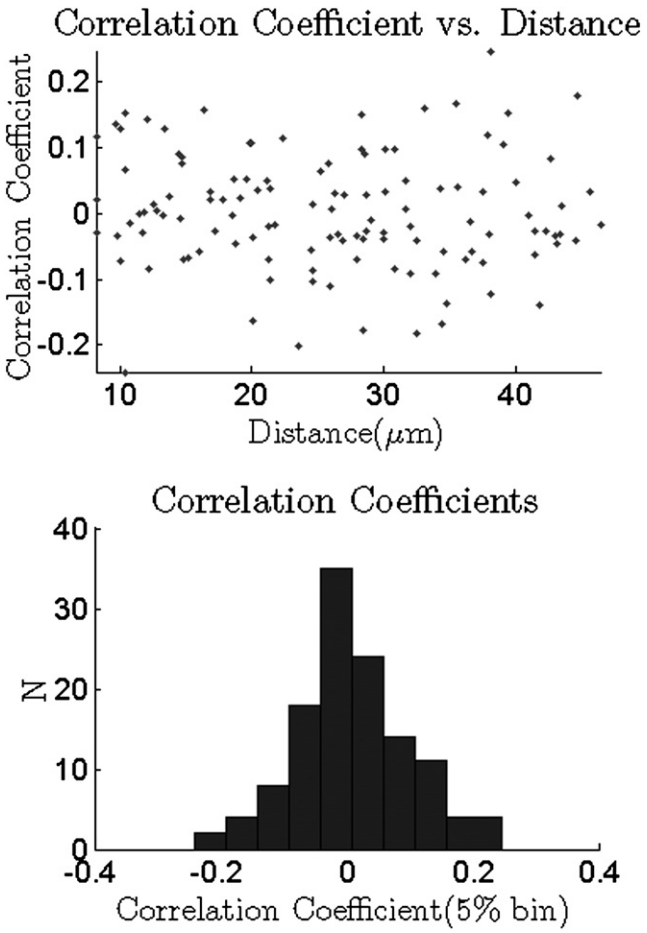

FIGURE 11 Correlation coefficients were computed for all pairs of oscillating hair bundles in a given field of view (*top*). Scatterplot displays correlation coefficients versus distance between bundles. No variation was found in degree of correlation between neighboring oscillators. Histogram of coefficients displays a center near 0% (*bottom*).

spontaneous oscillations in free-standing bundles, because these were shown to indicate an underlying active process.

Our experiments provided probability distributions of time intervals between the opening and closing of transduction channels, measured in a total of 373 spontaneously oscillating hair bundles. Data were pooled over different numbers of cells, to obtain comparisons of frequencies over both fine-grained and coarse-grained spatial scales. Histograms of data measured across different parts of the sacculus, and pooled from different epithelia, produced a broad and asymmetric distribution, with a peak oscillation period of 33 ms (+29 ms, −14 ms).

We also found that the distribution of frequencies of spontaneous oscillations did not follow a spatial pattern, tonotopic or otherwise, but seemed randomly distributed across the epithelium. This observation was consistent on several different scales of spatial distances, as measured in different sacculi and bullfrogs.

Thirdly, correlation coefficients measured between movements of neighboring bundles demonstrated that spontaneous oscillations in individual hair cells are uncorrelated. Insofar as the mechanical coupling element, i.e., otolithic membrane (88,89), was absent in these preparations, and the efferent fibers (90) innervating the hair cells were severed, the two elements most likely to impose any synchrony between oscillators were removed. However, we wanted to verify the absence of any additional mechanism intrinsic to the cells that could maintain a global phase and lead to some degree of correlation. Hence, any correlation that may arise between hair bundles under native conditions must be ascribed to the overlying membrane or other external mechanisms.

Finally, these experiments demonstrated the use of high-speed CMOS cameras as detectors of hair-bundle oscillation. This method allows for the measurement of as many as 20 cells in parallel, with a noise floor in the range of a few nanometers. This approach offers several advantages over other techniques, and opens up possibilities for further applications. The simultaneous tracking of multiple elements allows for a direct observation of correlations and phase-locking between individual oscillators. Secondly, by tracking many hair bundles in parallel, it speeds data acquisition and enables measurements of greater numbers of cells from a single preparation, an improvement important in studies where a statistical assessment is desirable. The high-speed nature of the camera is particularly useful for studying spontaneous motility, which exhibits fluctuations in frequency and phase, and thus does not lend itself to strobing techniques. We anticipate that our approach will be readily generalizable to other sensory organs in the bullfrog, and to sensory organs of other species.

CONCLUSION

We found that periods of spontaneous oscillations in the saccular epithelium were randomly distributed across different areas of the preparation, including that of the striolar region, and across different sacculi. The distribution was broad, with a peak period of 33 ms. Individual oscillations were uncorrelated with respect to their neighbors, as expected in free-standing hair bundles. This study established a methodology that allows for the time-resolved recording of many hair bundles in parallel, facilitating the acquisition of sufficient statistics to characterize their behavior across the whole epithelium.

We thank J. Landy for useful discussions about the probability density estimator. R. Williams-Garcia, A. Kao, and M. Webster provided helpful comments on the writing of the manuscript. With regard to the CMOS camera, we thank T. Takimizu, S. Kimura, and T. Onuma from Photron, and A. Cheng, for technical support and useful discussions.

This work was supported in part by National Science Foundation grant MRI-0723204.

REFERENCES

1. Hudspeth, A. J. 2000. Hearing. *In* Principles of Neural Science. E. R. Kandel, J. H. Schwartz, and T. M. Jessell, editors. McGraw-Hill, New York. 590–624.

2. Hudspeth, A. J., Y. Choe, A. D. Mehta, and P. Martin. 2000. Putting ion channels to work: mechanoelectrical transduction, adaptation, and amplification by hair cells. *Proc. Natl. Acad. Sci. USA*. 97:11765–11772.
3. Vollrath, M. A., K. Y. Kwan, and D. P. Corey. 2007. The micromachinery of mechanotransduction in hair cells. *Annu. Rev. Neurosci.* 30:339–365.
4. Chan, D. K., and A. J. Hudspeth. 2005. Ca^{2+} current-driven nonlinear amplification by the mammalian cochlea in vitro. *Nat. Neurosci.* 8:149–165.
5. Dallos, P. 1992. The active cochlea. *J. Neurosci.* 12:4575–4585.
6. Fettiplace, R., A. J. Ricci, and C. M. Hackney. 2001. Clues to the cochlear amplifier from the turtle ear. *Trends Neurosci.* 24:169–175.
7. Gold, T. 1948. Hearing II. The physical basis of the action of the cochlea. *Proc. R. Soc. Lond. B. Biol. Sci.* 135:492–498.
8. Hudspeth, A. 1997. Mechanical amplification of stimuli by hair cells. *Curr. Opin. Neurobiol.* 7:480–486.
9. Kennedy, H. J., M. G. Evans, A. C. Crawford, and R. Fettiplace. 2003. Fast adaptation of mechanoelectrical transducer channels in mammalian cochlear hair cells. *Nat. Neurosci.* 6:832–836.
10. Kennedy, H. J., M. G. Evans, A. C. Crawford, and R. Fettiplace. 2006. Depolarization of cochlear outer hair cells evokes active hair bundle motion by two mechanisms. *J. Neurosci.* 26:2757–2766.
11. LeMasurier, M., and P. G. Gillespie. 2005. Hair-cell mechanotransduction and cochlear amplification. *Neuron*. 48:403–415.
12. Manley, G. A. 2000. Cochlear mechanisms from a phylogenetic viewpoint. *Proc. Natl. Acad. Sci. USA*. 97:11736–11743.
13. Manley, G. A. 2001. Evidence for an active process and a cochlear amplifier in nonmammals. *J. Neurophysiol.* 86:541–549.
14. Nobili, R., F. Mammano, and J. Ashmore. 1998. How well do we understand the cochlea? *Trends Neurosci.* 21:159–167.
15. Ren, T., and P. G. Gillespie. 2007. A mechanism for active hearing. *Curr. Opin. Neurobiol.* 17:498–503.
16. Ricci, A. J., A. C. Crawford, and R. Fettiplace. 2000. Active hair bundle motion linked to fast transducer adaptation in auditory hair cells. *J. Neurosci.* 20:7131–7142.
17. Ricci, A. J., A. C. Crawford, and R. Fettiplace. 2002. Mechanisms of active hair bundle motion in auditory hair cells. *J. Neurosci.* 22:44–52.
18. Santos-Sacchi, J. 2003. New tunes from corti's organ: the outer hair cell boogie rules. *Curr. Opin. Neurobiol.* 13:459–468.
19. Stauffer, E. A., J. D. Scarborough, M. Hirono, E. D. Miller, K. Shah, et al. 2005. Fast adaptation in vestibular hair cells requires myosin-1c activity. *Neuron*. 47:541–553.
20. Benser, M. E., R. E. Marquis, and A. J. Hudspeth. 1996. Rapid, active hair bundle movements in hair cells from the bullfrog's sacculus. *J. Neurosci.* 16:5629–5643.
21. Denk, W., and W. W. Webb. 1992. Forward and reverse transduction at the limit of sensitivity studied by correlating electrical and mechanical fluctuations in frog saccular hair cells. *Hear. Res.* 60:89–102.
22. Howard, J., and A. J. Hudspeth. 1987. Mechanical relaxation of the hair bundle mediates adaptation in mechanoelectrical transduction by the bullfrog's saccular hair cell. *Proc. Natl. Acad. Sci. USA*. 84:3064–3068.
23. Martin, P., D. Bozovic, Y. Choe, and A. J. Hudspeth. 2003. Spontaneous oscillation by hair bundles of the bullfrog's sacculus. *J. Neurosci.* 23:4533–4548.
24. Martin, P., A. D. Mehta, and A. J. Hudspeth. 2000. Negative hair-bundle stiffness betrays a mechanism for mechanical amplification by the hair cell. *Proc. Natl. Acad. Sci. USA*. 97:12026–12031.
25. Crawford, A. C., and R. Fettiplace. 1985. The mechanical properties of ciliary bundles of turtle cochlear hair cells. *J. Physiol.* 364:359–379.
26. Martin, P., and A. J. Hudspeth. 1999. Active hair-bundle movements can amplify a hair cell's response to oscillatory mechanical stimuli. *Proc. Natl. Acad. Sci. USA*. 96:14306–14311.
27. Martin, P., A. J. Hudspeth, and F. Julicher. 2001. Comparison of a hair bundle's spontaneous oscillations with its response to mechanical stimulation reveals the underlying active process. *Proc. Natl. Acad. Sci. USA*. 98:14380–14385.
28. Duke, T., and F. Julicher. 2003. Active traveling wave in the cochlea. *Phys. Rev. Lett.* 90:158101–158104.
29. Eguiluz, V. M., M. Ospeck, Y. Choe, A. J. Hudspeth, and M. O. Magnasco. 2000. Essential nonlinearities in hearing. *Phys. Rev. Lett.* 84:5232–5235.
30. Magnasco, M. O. 2003. A wave traveling over a Hopf instability shapes the cochlear tuning curve. *Phys. Rev. Lett.* 90, 058101.
31. Nadrowski, B., P. Martin, and F. Julicher. 2004. Active hair-bundle motility harnesses noise to operate near an optimum of mechanosensitivity. *Proc. Natl. Acad. Sci. USA*. 101:12195–12200.
32. Tinevez, J. Y., F. Julicher, and P. Martin. 2007. Unifying the various incarnations of active hair-bundle motility by the vertebrate hair cell. *Biophys. J.* 93:4053–4067.
33. Camalet, S., T. Duke, F. Julicher, and J. Prost. 2000. Auditory sensitivity provided by self-tuned critical oscillations of hair cells. *Proc. Natl. Acad. Sci. USA*. 97:3183–3188.
34. Julicher, F., and J. Prost. 1997. Spontaneous oscillations of collective molecular motors. *Phys. Rev. Lett.* 78:4510–4513.
35. Goodyear, R. J., and G. P. Richardson. 2002. Extracellular matrices associated with the apical surfaces of sensory epithelia in the inner ear: molecular and structural diversity. *J. Neurobiol.* 53:212–227.
36. Vilfan, A., and T. Duke. 2003. Two adaptation processes in auditory hair cells together can provide an active amplifier. *Biophys. J.* 85:191–203.
37. Corey, D. P., and A. J. Hudspeth. 1983. Kinetics of the receptor current in bullfrog saccular hair cells. *J. Neurosci.* 3:962–976.
38. Denk, W., J. R. Holt, G. M. Shepherd, and D. P. Corey. 1995. Calcium imaging of single stereocilia in hair cells: localization of transduction channels at both ends of tip links. *Neuron*. 15:1311–1321.
39. Géléoc, G. S., G. W. Lennan, G. P. Richardson, and C. J. Kros. 1997. A quantitative comparison of mechanoelectrical transduction in vestibular and auditory hair cells of neonatal mice. *Proc Biol Sci.* 264:611–621.
40. Gillespie, P. G., R. A. Dumont, and B. Kachar. 2005. Have we found the tip link, transduction channel, and gating spring of the hair cell? *Curr. Opin. Neurobiol.* 15:389–396.
41. Gillespie, P. G., and R. G. Walker. 2001. Molecular basis of mechanosensory transduction. *Nature*. 413:194–202, (Journal Article Review England.).
42. Goodman, M. B., E. A. Lumpkin, A. Ricci, W. D. Tracey, M. Kernan, et al. 2004. Molecules and mechanisms of mechanotransduction. *J. Neurosci.* 24:9220–9222.
43. Howard, J., and A. J. Hudspeth. 1988. Compliance of the hair bundle associated with gating of mechanoelectrical transduction channels in the bullfrog's saccular hair cell. *Neuron*. 1:189–199.
44. Jaramillo, F., and A. J. Hudspeth. 1991. Localization of the hair cell's transduction channels at the hair bundle's top by iontophoretic application of a channel blocker. *Neuron*. 7:409–420.
45. Markin, V. S., and A. J. Hudspeth. 1995. Gating-spring models of mechanoelectrical transduction by hair cells of the internal ear. *Annu. Rev. Biophys. Biomol. Struct.* 24:59–83.
46. Pickles, J. O., and D. P. Corey. 1992. Mechanoelectrical transduction by hair cells. *Trends Neurosci.* 15:254–259.
47. Russell, I. J., M. Kossl, and G. P. Richardson. 1992. Nonlinear mechanical responses of mouse cochlear hair bundles. *Proc Biol Sci.* 250:217–227.
48. van Netten, S. M., and C. J. Kros. 2000. Gating energies and forces of the mammalian hair cell transducer channel and related hair bundle mechanics. *Proc Biol Sci.* 267:1915–1923.
49. Kachar, B., M. Parakkal, M. Kurc, Y. Zhao, and P. G. Gillespie. 2000. High-resolution structure of hair-cell tip links. *Proc. Natl. Acad. Sci. USA*. 97:13336–13341.

50. Tsuprun, V., R. J. Goodyear, and G. P. Richardson. 2004. The structure of tip links and kinocilial links in avian sensory hair bundles. *Biophys. J.* 87:4106–4112.

51. Batters, C., C. P. Arthur, A. Lin, J. Porter, M. A. Geeves, et al. 2004. Myo1c is designed for the adaptation response in the inner ear. *EMBO J.* 23:1433–1440.

52. Burlacu, S., W. D. Tap, E. A. Lumpkin, and A. J. Hudspeth. 1997. ATPase activity of myosin in hair bundles of the bullfrog's sacculus. *Biophys. J.* 72:263–271.

53. Cyr, J. L., R. A. Dumont, and P. G. Gillespie. 2002. Myosin-1c interacts with hair-cell receptors through its calmodulin-binding IQ domains. *J. Neurosci.* 22:2487–2495.

54. Gillespie, P. G., and D. P. Corey. 1997. Myosin and adaptation by hair cells. *Neuron.* 19:955–958.

55. Gillespie, P. G., and J. L. Cyr. 2004. Myosin-1c, the hair cell's adaptation motor. *Annu. Rev. Physiol.* 66:521–545.

56. Gillespie, P. G., M. C. Wagner, and A. J. Hudspeth. 1993. Identification of a 120 kD hair-bundle myosin located near stereociliary tips. *Neuron.* 11:581–594.

57. Hasson, T., P. G. Gillespie, J. A. Garcia, R. B. MacDonald, Y. D. Zhao, et al. 1997. Unconventional myosins in inner-ear sensory epithelia. *J. Cell Biol.* 137:1287–1307.

58. Holt, J. R., S. K. Gillespie, D. W. Provance, K. Shah, K. M. Shokat, et al. 2002. A chemical-genetic strategy implicates myosin-1c in adaptation by hair cells. *Cell.* 108:371–381.

59. Jacobs, R. A., and A. J. Hudspeth. 1990. Ultrastructural correlates of mechanoelectrical transduction in hair cells of the bullfrog's internal ear. *Cold Spring Harbor Symp. Quant. Biol.* 55:547–561.

60. Shepherd, G. M., D. P. Corey, and S. M. Block. 1990. Actin cores of hair-cell stereocilia support myosin motility. *Proc. Natl. Acad. Sci. USA.* 87:8627–8631.

61. Wu, Y. C., A. J. Ricci, and R. Fettiplace. 1999. Two components of transducer adaptation in auditory hair cells. *J. Neurophysiol.* 82:2171–2181.

62. Yamoah, E. N., and P. G. Gillespie. 1996. Phosphate analogs block adaptation in hair cells by inhibiting adaptation-motor force production. *Neuron.* 17:523–533.

63. Assad, J. A., and D. P. Corey. 1992. An active motor model for adaptation by vertebrate hair cells. *J. Neurosci.* 12:3291–3309.

64. Crawford, A. C., M. G. Evans, and R. Fettiplace. 1989. Activation and adaptation of transducer currents in turtle hair cells. *J. Physiol. (Lond.).* 419:405–434.

65. Eatock, R. A. 2000. Adaptation in hair cells. *Annu. Rev. Neurosci.* 23:285–314.

66. Eatock, R. A., D. P. Corey, and A. J. Hudspeth. 1987. Adaptation of mechanoelectrical transduction in hair cells of the bullfrog's sacculus. *J. Neurosci.* 7:2821–2836.

67. Fettiplace, R., and A. J. Ricci. 2003. Adaptation in auditory hair cells. *Curr. Opin. Neurobiol.* 13:446–451.

68. Holt, J. R., and D. P. Corey. 2000. Two mechanisms for transducer adaptation in vertebrate hair cells. *Proc. Natl. Acad. Sci. USA.* 97:11730–11735.

69. Holt, J. R., D. P. Corey, and R. A. Eatock. 1997. Mechanoelectrical transduction and adaptation in hair cells of the mouse utricle, a low-frequency vestibular organ. *J. Neurosci.* 17:8739–8748.

70. Hudspeth, A. J., and P. G. Gillespie. 1994. Pulling springs to tune transduction: adaptation by hair cells. *Neuron.* 12:1–9.

71. Metcalf, A. B., Y. Chelliah, and A. J. Hudspeth. 1994. Molecular cloning of a myosin I beta isozyme that may mediate adaptation by hair cells of the bullfrog's internal ear. *Proc. Natl. Acad. Sci. USA.* 91:11821–11825.

72. Shepherd, G. M., and D. P. Corey. 1994. The extent of adaptation in bullfrog saccular hair cells. *J. Neurosci.* 14:6217–6229.

73. Walker, R. G., and A. J. Hudspeth. 1996. Calmodulin controls adaptation of mechanoelectrical transduction by hair cells of the bullfrog's sacculus. *Proc. Natl. Acad. Sci. USA.* 93:2203–2207.

74. Koyama, H., E. R. Lewis, E. L. Leverenz, and R. A. Baird. 1982. Acute seismic sensitivity in the bullfrog ear. *Brain Res.* 250:168–172.

75. Lewis, E. R. 1988. Tuning in the bullfrog ear. *Biophys. J.* 53:441–447.

76. Smotherman, M. S., and P. M. Narins. 2000. Hair cells, hearing and hopping: a field guide to hair cell physiology in the frog. *J. Exp. Biol.* 203:2237–2246.

77. Christensen-Dalsgaard, J., and M. B. Jorgensen. 1988. The response characteristics of vibration-sensitive saccular fibers in the grassfrog, *Rana temporaria*. *J. Comp. Physiol. [A].* 162:633–638.

78. Christensen-Dalsgaard, J., and P. M. Narins. 1993. Sound and vibration sensitivity of VIIIth nerve fibers in the frogs *Leptodactylus albilabris* and *Rana pipiens pipiens*. *J. Comp. Physiol. [A].* 172:653–662.

79. Egert, D., and E. R. Lewis. 1995. Temperature-dependence of saccular nerve fiber response in the North American bullfrog. *Hear. Res.* 84: 72–80.

80. Lewis, E. R., R. A. Baird, E. L. Leverenz, and H. Koyama. 1982. Inner-ear-dye injection reveals peripheral origins of specific sensitivities. *Science.* 215:1641–1643.

81. Moffatt, A. J. M., and R. R. Capranica. 1976. Auditory sensitivity of the saccule in the American toad (*Bufo americanus*). *J. Comp. Physiol. [A].* 105:1–8.

82. Yu, X. L., E. R. Lewis, and D. Feld. 1991. Seismic and auditory tuning curves from bullfrog saccular and amphibian papillar axons. *J. Comp. Physiol. [A].* 169:241–248.

83. Le Goff, L., D. Bozovic, and A. J. Hudspeth. 2005. Adaptive shift in the domain of negative stiffness during spontaneous oscillation by hair bundles from the internal ear. *Proc. Natl. Acad. Sci. USA.* 102:16996–17001.

84. Fredrickson, L., A. Cheng, C. E. Strimbu, D. Bozovic, and K. Arisaka. 2008. The use of a CMOS camera to resolve nanometer displacements of hair cell stereocillia in the bullfrog sacculus. *Proc. SPIE.* 6859: 68591B-1–68591B-7.

85. Heintzmann, R., and G. Ficz. 2006. Breaking the resolution limit in light microcopy. *Brief. Funct. Genomics Proteomics.* 5:289–301.

86. Kozlov, A. S., T. Risler, and A. J. Hudspeth. 2007. Coherent motion of stereocilia assures the concerted gating of hair-cell transduction channels. *Nat. Neurosci.* 10:87–92.

87. Popper, A. N. 1981. Comparative scanning electron microscopic investigations of the sensory epithelia in the teleost sacculus and lagena. *J. Comp. Neurol.* 200:357–374.

88. Hillman, D. E., and E. R. Lewis. 1971. Morphological basis for a mechanical linkage in otolithic receptor transduction in the frog. *Science.* 174:416–419.

89. Bechara Kachar, B., M. Parakkal, and J. Fex. 1990. Structural basis for mechanical transduction in the frog vestibular sensory aparatus: I. The otolithic membrane. *Hear. Res.* 45:179–190.

90. Manley, G. A., and C. Koppl. 1998. Phylogenetic development of the cochlea and its innervation. *Curr. Opin. Neurobiol.* 8:468–474.